Electron-phonon coupling at metal surfaces

2002 J. Phys.: Condens. Matter 14 5959

(http://iopscience.iop.org/0953-8984/14/24/306)

INSTITUTE OF PHYSICS PUBLISHING JOURNAL OF PHYSICS: CONDENSED MATTER

J. Phys.: Condens. Matter **14** (2002) 5959–5977 PII: S0953-8984(02)36745-6

Electron–phonon coupling at metal surfaces

B Hellsing[1], **A Eiguren**[2] **and E V Chulkov**[1,2]

[1] Donostia International Physics Center (DIPC), Paseo de Manuel Lardizabal, 4, 20018 San Sebastián/Donostia, Spain

[2] Departmento de Física de Materiales and Centro Mixto CSIC-UPV/EHU, Facultad de Ciencias Químicas, Universidad del Pais Vasco/Euskal Herriko Unibertsitatea, Apdo 1072, 20018 San Sebastián/Donostia, Basque Country, Spain

Received 9 May 2002
Published 31 May 2002
Online at stacks.iop.org/JPhysCM/14/5959

Abstract

Chemical reactions at metal surfaces are influenced by inherent dissipative processes which involve energy transfer between the conduction electrons and the nuclear motion. We shall discuss how it is possible to model this electron–phonon coupling in order to estimate its importance. A relevant quantity for this investigation is the lifetime of surface-localized electron states. A surface state, quantum well state or surface image state is located in a surface-projected bandgap and becomes relatively sharp in energy. This makes a comparison between calculations and experimental data most attractive, with a possibility of resolving the origin of the lifetime broadening of electron states. To achieve more than an order of magnitude estimate we point out the importance of taking into account the phonon spectrum, electron surface state wavefunctions and screening of the electron–ion potential.

1. Introduction

During the last two decades an impressive development of experimental techniques has been achieved to even pin down the fundamental interactions in solids, such as the electron–electron (e–e) and the electron–phonon (e–p) interactions. It is obvious that a detailed understanding of these interactions is crucial in the field of nanoscale physics, where quantum size effects are important and the e–e and e–p interactions inevitably will limit the lifetime of excited one-electron states. In surface chemistry a reaction often proceeds via an intermediate electronically excited state. A relevant question is then whether the lifetime of this excited state is compatible with the time it takes for the reactants to complete the reaction, or at least long enough that a significant fraction will. For this reason it is important to find the parameters that determine the lifetime of the excitation. The decay channel of an excited electronic state via excitations of secondary electrons has been investigated theoretically in detail for many systems [1–3]. The aim of this paper is not to present a complete review but rather to discuss, with some examples, how we can proceed theoretically in order to estimate, or perform a

real calculation of, the lifetimes of surface states taking into account the lattice vibrations in solids—the e–p scattering mechanism. The e–p coupling may also play an important role in damping atomic motion on surfaces. If an adsorbate has excess kinetic or vibrational energy, its motion could be damped due to excitations of low-energy electron–hole pairs—electronic friction [4–12]. This phenomenon will not be considered here.

Today, several ways to experimentally investigate lifetimes of surface-localized electron states have been presented: angular-resolved photoemission electron spectroscopy (ARPES) [13–19], two-photon photoemission (2PPE) techniques [20, 21], a time-resolved 2PPE technique for direct determination of excitation lifetimes [22–33] and different methods based on scanning tunnelling spectroscopy [34–40].

Photoemission studies of the Cu(111) sp-derived surface state have been presented with the focus on the temperature dependence of the emission line width [41, 42]. Matzdorf *et al* [41] pointed out that the temperature dependence was not due to a Debye–Waller effect and McDougall *et al* [42] convincingly showed that the linear temperature dependence of the width was consistent with an e–p coupling mechanism. More recently, similar observations have been reported for overlayer systems where the clean surface state is replaced by overlayer-localized quantum well states (QWSs) [43–47]. A line shape analysis of the photoemission spectra has been presented for the system of one monolayer (ML) of Na adsorbed on Cu(111) [44].

The outline of the paper is as follows. First, in section 2, we present, in some detail, a theoretical derivation of the relevant formulae to be used in a calculation of the phonon-induced lifetime broadening. Next, in section 3, we present some simple models and more serious attempts to calculate the phonon-induced lifetime broadening. Finally, in section 4, we make some concluding remarks and look into the future.

2. Self-energy

We consider that $\epsilon(\vec{k})$ represent the one-electron energies in absence of the e–p interaction. Turning on the e–p interaction, electron scattering takes place. The existence of quasi-particles reveals itself as peaks in the spectral function $A(\omega, \vec{k})$. The peak width gives us the inverse lifetime of the quasi-particle and is referred to as the lifetime broadening.

The general formulation of the lifetime broadening of an electron state due to the e–p interaction in terms of Green function and self-energy formalism proceeds as follows. In a photoemission experiment, the contribution from the e–p interaction to the observed peak width, referring to a particular momentum $\vec{k}$ and energy relative to the Fermi level ω, is determined by the spectral function $A(\omega, \vec{k})$ given by the imaginary part of the Green function.

$$A(\omega, \vec{k}) = \frac{1}{\pi} \frac{|\mathrm{Im}\ \sum_{\mathrm{ep}}(\omega, \vec{k})|}{[\omega - \xi_{\vec{k}} - \mathrm{Re}\ \sum_{\mathrm{ep}}(\omega, \vec{k})]^2 + [\mathrm{Im}\ \sum_{\mathrm{ep}}(\omega, \vec{k})]^2}, \tag{1}$$

where $\xi_{\vec{k}} = \epsilon(\vec{k}) - \epsilon_F$ is the unperturbed one-electron energy relative to the Fermi level and $\sum_{\mathrm{ep}}$ is the appropriate self-energy due to the e–p interaction.

2.1. Lifetime broadening Γ_{ep}

In the case of weak coupling, ω in the argument of the self-energy can be replaced by the unperturbed energy $\xi_{\vec{k}}$ and the spectral function $A(\omega, \vec{k})$ in equation (1) takes the form of a pure Lorentzian function with respect to the dependence of ω with the full width at half maximum (FWHM) given by $\Gamma_{\mathrm{ep}} = 2|\mathrm{Im}\ \sum_{\mathrm{ep}}(\xi_{\vec{k}}, \vec{k})|$. As it is our intention to later on consider a metal slab we introduce the following form of the one-electron wavefunction and energy:

$$\psi_{n,\vec{k}_\parallel}(z,\vec{x}) = \frac{1}{\sqrt{A}}\phi_n(z)\mathrm{e}^{\mathrm{i}\vec{k}_\parallel\cdot\vec{x}} \qquad \epsilon_n(\vec{k}_\parallel) = \epsilon_n^0 + \hbar^2 k_\parallel^2/2m_n, \tag{2}$$

where n is the band index, $\vec{k}_\parallel$ the momentum parallel to the surface and A the surface area. In the following we shall suppress the $\parallel$ index. The z coordinate is along the surface normal and $\vec{x}$ in the surface plane.

Now, the fingerprint of the e–p coupling is its temperature dependence. If we do not consider electron states within a typical phonon energy from the Fermi level this T-dependence is simply due to the T-dependence of the number of phonons. To calculate Γ_{ep} we consider the lowest-order contribution to the self-energy represented by the diagram in figure 1. Higher-order diagrams, including multi-phonon processes, are believed to be of minor importance [48–51]. According to the rules of Feynman diagrams, the one-phonon self-energy pictured in figure 1 in terms of the temperature-dependent Matsubara Green functions of the phonon $\mathcal{D}$ and electron $\mathcal{G}$ is written [51]

$$\widetilde{\sum}_{\mathrm{ep}}(\mathrm{i}p,\vec{k}_i) = -\sum_{\nu,\vec{q},f}|g^\nu_{i,f}(\vec{q})|^2\frac{1}{\beta}\sum_{n=-\infty}^{+\infty}\mathcal{D}_\nu(\vec{q},\mathrm{i}\omega_n)\mathcal{G}_f(\vec{k}_i+\vec{q},\mathrm{i}p+\mathrm{i}\omega_n), \tag{3}$$

where $\mathrm{i}p$ (satisfying $\exp(\mathrm{i}p\beta) = -1$) and $\vec{k}_i$ are the initial imaginary energy and the parallel momentum of the electron state, $g^\nu_{i,f}$ the static e–p coupling function, ν and $\vec{q}$ denote the phonon mode and phonon wavevector and f is the band index. The Matsubara summation is, as indicated in equation (3), over all integers n and $\omega_n = 2n\pi/\beta$, where $\beta = 1/(k_BT)$ [51]. The e–p coupling function includes the matrix element between the initial (i) and final (f) electron bands. The matrix element involves a z-integration (see equation (2)).

$$g^\nu_{i,f}(\vec{q}) = \sqrt{\frac{1}{2MN\omega_\nu(\vec{q})}}\langle f|\sum_\mu \vec{\epsilon}_{\vec{q}\nu}(\vec{R}_\mu)\cdot\vec{\nabla}_{\vec{R}_\mu}\tilde{V}^\mu_q|i\rangle. \tag{4}$$

We neglect the frequency dependence of the coupling function g_ν and thus consider the static screening of the electron–ion potential. This approximation is acceptable since the phonon frequencies are in general small in comparison with the energies of the scattered electrons. The coupling function in equation (4) is the result of the standard first-order expansion of the screened electron–ion potential, $\tilde{V}^\mu_q$, with respect to the vibrational coordinate $\vec{R}_\mu$. N is the number of ions in each layer, M is the ion mass, μ is the layer index and $\vec{\epsilon}_{\vec{q}\nu}(\vec{R}_\mu)$ are the phonon polarization vectors. We insert the unperturbed Green functions of both the phonon and the electron in equation (3). Performing the Matsubara summation, which can be evaluated by a contour integration in the complex frequency plane, yields the result [51]

$$\frac{1}{\beta}\sum_{n=-\infty}^{+\infty}\frac{2\omega_\nu(\vec{q})}{\omega_n^2+\omega_\nu^2(\vec{q})}\frac{1}{\mathrm{i}p+\mathrm{i}\omega_n-\xi_{f,\vec{k}_i+\vec{q}}} = \frac{1+n(\omega_\nu)-f(\xi_{f,\vec{k}_i+\vec{q}})}{\mathrm{i}p-\xi_{f,\vec{k}_i+\vec{q}}-\omega_\nu} + \frac{n(\omega_\nu)+f(\xi_{f,\vec{k}_i+\vec{q}})}{\mathrm{i}p-\xi_{f,\vec{k}_i+\vec{q}}+\omega_\nu}, \tag{5}$$

where f and n are the electron and phonon distribution functions, respectively, $\omega_\nu \equiv \omega_\nu(\vec{q})$ and $\xi_{f,\vec{k}_i+\vec{q}} = \epsilon_f^0 + \hbar^2|\vec{k}_i+\vec{q}|^2/2m_f - \epsilon_F$. In order to obtain the appropriate retarded self-energy $\sum_{\mathrm{ep}}$ we take the limit $\mathrm{i}p \to \omega + \mathrm{i}\delta$ and insert the result of equation (5) into (3). We thus obtain

$$\sum_{\mathrm{ep}}(\omega,\vec{k}_i) = \sum_{\nu,\vec{q},f}|g^\nu_{i,f}(\vec{q})|^2\left[\frac{1+n(\omega_\nu)-f(\xi_{f,\vec{k}_i+\vec{q}})}{\omega-\xi_{f,\vec{k}_i+\vec{q}}-\omega_\nu+\mathrm{i}\delta} + \frac{n(\omega_\nu)+f(\xi_{f,\vec{k}_i+\vec{q}})}{\omega-\xi_{f,\vec{k}_i+\vec{q}}+\omega_\nu+\mathrm{i}\delta}\right]. \tag{6}$$

The phonon-induced lifetime broadening $\Gamma_{\mathrm{ep}} = 2|\mathrm{Im}\sum_{\mathrm{ep}}|$ is then

$$\begin{aligned}\Gamma_{\mathrm{ep}}(\omega,\vec{k}_i) = 2\pi\sum_{\nu,\vec{q},f}|g^\nu_{i,f}(\vec{q})|^2\{&[1+n(\omega_\nu)-f(\xi_{f,\vec{k}_i+\vec{q}})]\delta(\omega-\xi_{f,\vec{k}_i+\vec{q}}-\omega_\nu)\\ &+[n(\omega_\nu)+f(\xi_{f,\vec{k}_i+\vec{q}})]\delta(\omega-\xi_{f,\vec{k}_i+\vec{q}}+\omega_\nu)]\}.\end{aligned} \tag{7}$$

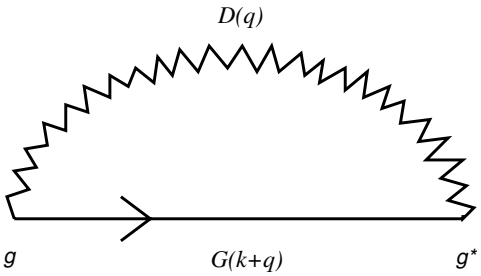

Figure 1. Schematic drawing of the lowest-order self-energy diagram representing the e–p interaction. $\mathcal{G}$ and $\mathcal{D}$ are the Matsubara Green functions of the electron and the phonon, respectively, and g is the e–p coupling function given in equation (4).

This result can also be obtained by using the golden rule, evaluating the net flow of electrons into the hole state [50]. Having a photoemission experiment in mind, the phonon-induced lifetime of a created hole with a binding energy $|\omega|$ and parallel momentum $\vec{k}_i$ then has two contributions. The first term in square parentheses of equation (7) represents phonon absorption and the second term phonon emission. We see from equation (7) that for a deep hole at zero temperature ($f = 1$ and $n = 0$) the first term is zero and only phonon emission is possible.

To relate to a conceptually simpler picture of the phonons we introduce the Eliashberg function $\alpha^2 F(\omega)$ [52], which is the phonon density of states weighted by the e–p coupling function g,

$$\alpha^2 F_{\vec{k}_i}(\omega) = \sum_{\nu,\vec{q},f} |g^{\nu}_{i,f}(\vec{q})|^2 \delta(\omega - \omega_\nu(\vec{q}))\delta(\epsilon_f - \epsilon_i), \tag{8}$$

where the last delta function indicates that we consider the quasi-elastic approximation, neglecting the change of the energy of the scattered electron due to absorption or emission of a phonon. Thus we can write $\Gamma_{\rm ep}$ as an integral over phonon energies. If we consider an initial hole state $(\omega, \vec{k}_i)$ and split the phonon absorption and emission processes into two separate terms (see figure 2), we write

$$\Gamma_{\rm ep}(\omega, \vec{k}_i) = 2\pi \left\{ \int_0^{\omega_m} \alpha^2 F_{\vec{k}_i}(\omega - \omega'')[1 + n(\omega - \omega'') - f(\omega'')]\, \mathrm{d}(\omega - \omega'') + \int_0^{\omega_m} \alpha^2 F(\omega' - \omega)[f(\omega') + n(\omega' - \omega)]\, \mathrm{d}(\omega' - \omega) \right\}, \tag{9}$$

where ω_m is the maximum phonon frequency. Changing variables, $\epsilon = \omega' - \omega$ in the first integral and $\epsilon = \omega - \omega''$ in the second, we obtain the result

$$\Gamma_{\rm ep}(\omega, \vec{k}_i) = 2\pi \int_0^{\omega_m} \alpha^2 F_{\vec{k}_i}(\epsilon)[1 + 2n(\epsilon) + f(\omega + \epsilon) - f(\omega - \epsilon)]\, \mathrm{d}\epsilon. \tag{10}$$

From equation (10) we easily obtain the $T = 0$ result ($\Rightarrow n = 0$) for $\Gamma_{\rm ep}$ as a function of hole binding energy $|\omega|$.

$$\Gamma_{\rm ep}(\omega, \vec{k}_i) = 2\pi \int_0^{|\omega|} \alpha^2 F_{\vec{k}_i}(\epsilon)\, \mathrm{d}\epsilon. \tag{11}$$

We close this section by connecting to the mass enhancement parameter λ. The e–p interaction will introduce a shift and a broadening of the unperturbed one-electron energies $\epsilon_n(\vec{k}) = \epsilon_n^0 + \hbar^2 k^2/2m_n$, where n is the band index and $\vec{k}$ is the parallel momentum vector in our slab. The broadening is determined by the imaginary part of the self-energy, while the real

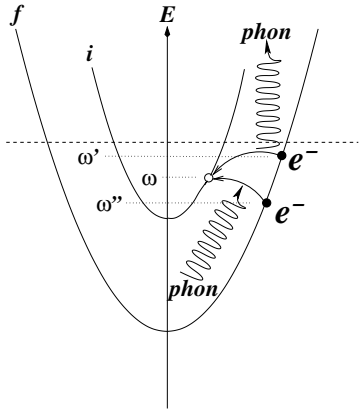

Figure 2. Schematic drawing of the phonon-mediated interband scattering from a band f (final state of the hole) to the band i (initial state of the hole) with energy ω. Both phonon emission and absorption are pictured.

part determines the shift. Neglecting the imaginary part, the shifted energies are given by the self-consistent solution of the equation

$$E_n(\vec{k}) - \epsilon_F = \epsilon_n(\vec{k}) - \epsilon_F + \mathrm{Re} \sum_{\mathrm{ep}} (E_n(\vec{k}) - \epsilon_F, \vec{k}). \tag{12}$$

If we assume that the one-electron energies retain their parabolic momentum dependence and introduce an effective electron band mass m_n^* we have

$$\frac{m}{m_n^*(\vec{k})} = \frac{\partial E_n(\vec{k})}{\partial \epsilon_n(\vec{k})}. \tag{13}$$

We then evaluate the derivative in equation (13) from (12) and neglect as usually [51] the $\vec{k}$ dependence of the self-energy in comparison with the ω dependence. This yields the result

$$m_n^*(\vec{k}) = m\left(1 - \frac{\partial \mathrm{Re} \sum_{\mathrm{ep}}(\omega, \vec{k}_n)}{\partial \omega}\right) \equiv m(1 + \lambda(\vec{k}_n)), \tag{14}$$

where we have introduced the mass enhancement parameter λ. We want to point out here that the assumed weak momentum dependence is not justified for the intraband scattering as in this case the band energies can be comparable to the phonon energies near the $\bar{\Gamma}$-point for acoustic phonon modes. However, for the interband scattering equation (14) should hold if the final-state band energies are much greater than the phonon energies. This is certainly fulfilled considering a hole in the surface state band of for example Cu(111) and Ag(111).

Expressing the derivative of the real part of the self-energy in terms of the Eliashberg function [51], λ is just the first reciprocal moment of the Eliashberg function

$$\lambda(\vec{k}_i) = 2 \int_0^{\omega_m} \frac{\alpha^2 F_{\vec{k}_i}(\omega)}{\omega} \, \mathrm{d}\omega. \tag{15}$$

If the high-T limit ($k_B T \gg \hbar\omega_m$) of equation (10) is considered, Grimvall [50] has pointed out a very useful result which enables an experimental determination of the mass enhancement parameter

$$\Gamma_{\mathrm{ep}}(\omega, \vec{k}_i) = 2\pi \lambda(\vec{k}_i) k_B T. \tag{16}$$

We thus conclude that the Eliashberg function $\alpha^2 F$ is a basic function to calculate. Given this function most of the interesting quantities can be calculated, such as the temperature and also binding energy dependence of the lifetime broadening and the mass enhancement parameter. However, this is no simple task, as all the physics connected to the e–p interaction is buried in $\alpha^2 F$, the phonon dispersion relation, phonon polarization vectors, one-electron wavefunctions and, last but not least, the gradient of the screened electron–ion potential—the deformation potential.

3. Calculations

In this section we present results from numerical calculations of the phonon-induced lifetime broadening $\Gamma_{\rm ep}$ for the QWS and the lowest image state (IS) for 1 ML Na on Cu(111). We also discuss broadening of the surface states of the clean noble metal surfaces Cu(111) and Ag(111). In the case of the QWS we shall present some improvements of previous published results [44]. First, however, we summarize and comment on some estimates based on simple models that have been presented in the literature recently.

3.1. Simple models

Several experimental studies, with the aim of estimating the lifetime broadening of surface states due to the e–p coupling, have been based on a simple phonon Debye model [17, 36, 42, 45, 56, 57]. For this reason let us briefly discuss this approach and make some comments. Assuming we have an experimentally determined λ value, we shall consider some Debye models in order to estimate the lifetime broadening at zero temperature ($T = 0$). For the phonon-induced decay of a surface-localized state, in principle both bulk and surface phonons might contribute. For this reason we apply three-dimensional, two-dimensional and also mixed $3D + 2D$ phonon models. For the pure two-dimensional phonon model we also include the case when including second-order Feynman diagrams [58] (nesting of two first-order diagrams shown in figure 1).

We denote the four Debye models $3D$, $2D_1$, $2D_2$ and $3D + 2D_1$, where the lower index refers to including first- and second-order diagrams. In the mixed $3D + 2D_1$ model we add to the $3D$ model a Rayleigh mode. Referring to the Eliashberg function in equation (8) we assume the e–p coupling function to be a constant and thus $\alpha^2 F$ is proportional to the phonon density of states. The Eliashberg functions of the models take the following forms:

$$\begin{aligned}
&\lambda(\omega/\omega_{DB})^2, && (3D)\\
&(\lambda/2)(\omega/\omega_{DS}), && (2D_1)\\
&(\lambda/\pi)\omega\Big/\sqrt{\omega_{DS}^2-\omega^2}, && (2D_2)\\
&\lambda(\omega/\omega_{DB})^2+(\lambda_R/2)(\omega/\omega_R)\theta(\omega_R-\omega), && (3D+2D_1),
\end{aligned} \tag{17}$$

where the lower indices DB, DS and R refer to bulk Debye, surface Debye and Rayleigh mode. In the case when the hole binding energy exceeds ω_{DB}, ω_{DS} and ω_R we calculated $\Gamma_{\rm ep}$ ($T = 0$) applying equation (11). In the table we show the results for the surface state of Cu(111) and Ag(111) at the $\bar{\Gamma}$-point.

When comparing these estimates we find a quite small spread of values, $\Gamma_{\rm ep} \approx 5$–$8$ and 3–5 meV, respectively for Cu(111) and Ag(111). In a real calculation of $\Gamma_{\rm ep}$, we determine the values as 6.9 and 3.8 meV [71]. We can thus conclude that, having a measured λ-value and some information about the phonon spectrum, a reasonable estimate of $\Gamma_{\rm ep}$ seems possible.

Table 1. Debye model estimates of Γ_{ep} ($T = 0$) in meV for the surface states of Cu(111) and Ag(111) at the $\bar{\Gamma}$-point. $\lambda_B = \lambda_R, \lambda = 0.14$ (Cu(111)) and 0.13 (Ag(111)), $\omega_{DB} = \omega_{DS} = 27$ meV (Cu(111)) and 18 meV (Ag(111)), $\omega_R = 13$ meV (Cu(111)) and 10 meV (Ag(111)). In the last column we give our calculated values (see section 3.3) presented in [71].

	$3D$	$2D_1$	$2D_2$	$3D + 2D_1$	Calc.
Cu(111)	7.9	5.9	7.6	5.4	6.9
Ag(111)	4.9	3.7	4.7	3.5	3.8

Lately, large λ-values have been reported from photoemission measurements for multilayer films, such as Ag/Fe(100) [17,45,59] and Ag/V(100) [46,47]. As pointed out in [59] one has to be careful when analysing the line shape of the distinct peaks in the normal photoemission spectra of the system Ag/Fe(100). As a real bandgap of the Fe(0001) surface does not exist, but rather a hybridization gap, part of the peak width is related to resonance broadening. The physics responsible for this broadening is that the wavefunction of the overlayer state does not decay exponentially into the substrate but has the character of an extended Bloch state with an enhanced energy-dependent amplitude in the overlayer region. Approximately, these resonances appear when the layer thickness corresponds to an integer number of half electron wavelengths. However, as we have seen in the previous section, the phonon-induced broadening has a characteristic linear high-temperature dependence, which in principle makes it possible to distinguish the e–p broadening from resonance broadening.

A model calculation has been presented to explain the experimental data for Ag/V(100) [46, 47]. The theoretical approach reveals an attempt to definitely go beyond the Debye model. However, when it comes to calculations rather drastic approximations are made. In the light of the general derivations of formulae for the lifetime broadening Γ_{ep} given in the previous section we want to stress two key aspects, (i) the phonon spectrum and (ii) the so-called rigid-ion approximation (RIA). First, having a closer look at the e–p coupling function in equation (4) we realize that what drives the scattering of electrons into the hole state, limiting its lifetime, is the change of the electron–ion potential as the ions vibrate. The phonon polarization vector, $\vec{\epsilon}_{\vec{q}\nu}(\vec{R}_\mu)$, of each phonon eigenmode $(\vec{q}\,\nu)$ gives the phonon amplitude over the ions of the system. Furthermore, as the square of the coupling function g enters Γ_{ep}, an explicit reciprocal frequency factor appears for the mode. We thus conclude that information about the phonon modes will determine the part of real space contributing to the integration represented by the matrix element in equation (4). Secondly, if, as usually assumed, the perturbation caused by the moving ions is local, due to the efficient screening in metals, we can assume the local valence charge to follow the ion motion rigidly. This leads to the so-called RIA [50].

$$\begin{aligned} V_{ie}(\vec{R}_j^0 + \vec{u}_j; \vec{r}) - V_{ie}(\vec{R}_j^0; \vec{r}) &\approx V_{ie}(\vec{R}_j^0 + \vec{u}_j - \vec{r}) - V_{ie}(\vec{R}_j^0 - \vec{r}) \\ &\approx \vec{u}_j \cdot \vec{\nabla}_{\vec{R}_j} V_{ie}(\vec{R}_j^0 - \vec{r}) = -\vec{u}_j \cdot \vec{\nabla}_{\vec{r}} V_{ie}(\vec{R}_j^0 - \vec{r}), \end{aligned} \tag{18}$$

where $\vec{R}_j^0$ is the equilibrium position of the ion labelled j and $\vec{u}_j$ the vibrational amplitude. In short RIA then yields

$$\vec{\nabla}_{\vec{R}_j} V_{ie}(\vec{R}_j^0 - \vec{r}) = -\vec{\nabla}_{\vec{r}} V_{ie}(\vec{R}_j^0 - \vec{r}). \tag{19}$$

Thus, the gradient of the screened electron–ion potential is not to be confused with the gradient of the full effective crystal one-electron potential, $\vec{\nabla}_{\vec{r}} V_{eff}(\vec{R}, \vec{r})$. The RIA has meaning if we consider the screened individual electron–ion potential, V_{ei}. This means that even if $V_{eff}(\vec{R}, \vec{r})$ varies strongly within a short-range interface region, this does not imply that the phonon-induced electron scattering is necessarily enhanced in this region. Connecting to

point (i) discussed above, this is the case *only* if there is an important phonon mode localized to this region.

In the work by Kralj *et al* [47], the overlayer system with 1–8 ML of Ag on top of a V(100) surface was considered. It is argued that it is appropriate to evaluate the e–p coupling matrix element at the film–vacuum interface, referring to the step in the effective one-electron potential. Furthermore, the frequency of the vibrating interface is assumed to be independent of the number of layers. However it is well known from experimental studies of overlayer structures, for example electron energy loss spectroscopy (EELS) studies of 1–2 ML of Li on Mo(110) [60] and helium atom scattering (HAS) of 1–20 ML of Na on Cu(100) [61], that nearly dispersionless open-ended 'organ pipe' modes exist in the thin overlayer. Increasing the number of layers, the number of modes increases with gradually lower frequencies. Thus, referring to the general discussion above, in order to seriously interpret the observed variation of the e–p interaction (measured λ parameter) as a function of the number of overlayers, information about the phonons of the system is crucial.

3.2. Na/Cu(111)

Recently, an experimental and theoretical study of the phonon-induced lifetime broadening of the occupied QWS of the system of 1 ML Na on Cu(111) was presented [44]. Here we shall add results for the broadening of an IS, reflecting the lifetime of an electron in the first excited state at the $\bar{\Gamma}$-point of the surface Brillouin zone. In figure 3 we show the QWS and IS bands. Two improvements in the calculations in comparison with [44] are made.

(i) *One-electron states derived from a slab calculation.* The slab model potential is constructed in line with the scheme by Chulkov *et al* [62–64]. The calculated QWS wavefunction is in good agreement with *ab initio* calculations [65] and the electron spectra close to experiment.

(ii) *A full three-dimensional integration of the e–p matrix elements with an ab initio deformation potential* ($\partial V_{ei}/\partial R_z$), which enables us to obtain the real-space range of the perturbation caused by the vibrating Na ions.

The phonons are modelled as follows. According to He scattering experiments on the system of 1 ML Na on Cu(100) [61], the phonon dispersion relation is flat, referring to the phonon energy versus momentum parallel to the surface. Furthermore, the observed vibrational modes are consistent with the 'organ pipe' type of modes normal to the surface [61]. Assuming the conditions are similar for 1 ML of Na on Cu(111), we adopt the Einstein model for the transverse overlayer vibrational mode polarized normal to the surface with an energy denoted $\hbar\Omega_o$.

The e–p coupling includes intraband and interband scattering. For the two separately investigated states, the QWS hole and the IS electron at the $\bar{\Gamma}$-point, intraband scattering only involves phonon emission for the QWS, while for the IS only phonon absorption. Interband transitions will include both phonon absorption and emission. In the case of the decay of the IS electron at the $\bar{\Gamma}$-point (parallel electron momentum equal to zero), the narrow energy window for the final states, given by twice the phonon energy, is also shown in figure 3.

Important quantities for a theoretical estimate of $\Gamma_{\rm ep}$ are the deformation potential $\partial V_{ei}/\partial R_z$ and the vibrational energy $\hbar\Omega_0$. We evaluate the deformation potential and the vibrational energy from a *first-principles* density functional theory (DFT) calculation [66, 67] using the generalized gradient approximation for the exchange–correlation functional [68], applying a plane wave basis and ultra-soft pseudo-potentials [69] for both Na and Cu [44, 65].

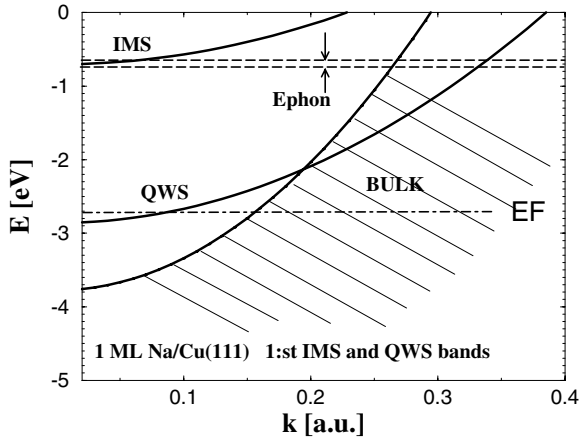

Figure 3. The one-electron bands of the QWS and the first IS for the system of 1 ML Na on Cu(111). Energies are given with respect to the vacuum level. The shaded region shows the region of the bulk bands. The region denoted Ephon shows the energy range of possible final states for scattered IS electrons.

The local deformation potential is calculated as

$$\partial V_{ei}(R_z = 0; z, \vec{x})/\partial R_z \approx [V_{DFT}(R_z = \delta Q; z, \vec{x}) - V_{DFT}(R_z = 0; z, \vec{x})]/\delta Q, \tag{20}$$

where $V_{DFT}(R_z = 0; z, \vec{x})$ and $V_{DFT}(R_z = \delta Q; z, \vec{x})$ is the local self-consistent effective one-electron potential, when the Na monolayer is in the relaxed equilibrium ground state and when it has been rigidly displaced a typical vibrational amplitude $\delta Q = 0.1$Å in the normal direction away from the copper substrate, respectively. Below we show that this deformation potential is actually confined within a radius less than half the nearest-neighbour distance in the monolayer. We want to point out that here we calculate the true deformation potential, not applying the RIA. The deformation of the electron–ion potential, as the Na atoms vibrate (equation (20)), is taken into account, as we know from detailed electron structure studies [65] that there is a substantial charge transfer from the Na overlayer to the copper substrate. This charge transfer is responsible for the Na-induced 2 eV decrease of the work function. In this way we include the dynamics of the screening of the ion–electron potential.

Applying a total-energy analysis we determined the vibrational energy $\hbar\Omega_0 = 21$ meV [44]. For Na on Cu(111) the vibrational energy has only been measured in the coverage range 0–0.35 ML and found to be rather constant, ∼21 meV [70]. Experimental data are available for 1 ML Na on Cu(100), and in this case the vibrational energy is $\hbar\Omega_0 = 18$ meV [61].

Due to the Einstein phonon approximation the e–p coupling function in equation (4) simplifies considerably. The binding energy of the QWS hole is about 100 meV and the excitation energy (relative to the Fermi level) of the IS electron is 2 eV. Thus, for any reasonable temperature the final states for the IS electron will be unoccupied and the final states of the QWS hole will be occupied. The temperature is thus completely determined by the phonon occupation numbers $n(\Omega_0)$. For the QWS hole decay we obtain

$$\Gamma_{\rm ep}^{QWS} = \frac{n_a}{2\hbar M\Omega_0}\left\{m_i^*|\mathcal{M}_{ii}|^2[1 + n(\Omega_0)] + \sum_f m_f^*|\mathcal{M}_{if}|^2[1 + 2n(\Omega_0)]\right\}, \tag{21}$$

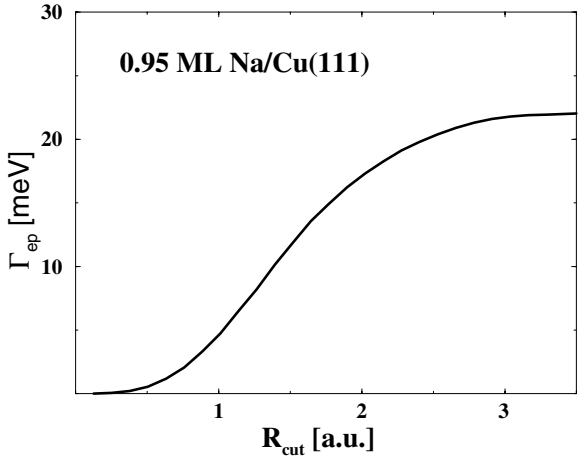

Figure 4. The phonon-induced lifetime broadening of the QWS at the $\bar{\Gamma}$-point calculated as a function of a cut-off radius of the radial part of the $\vec{x}$ integration in equation (23).

where m_i^* is the QWS electron band mass, m_f^* the final-state band mass, n_a the surface density of Na atoms and M the Na atom mass. For the IS electron decay we have

$$\Gamma_{\rm ep}^{IS} = \frac{n_a}{2\hbar M\Omega_0}\left\{m_i^*|\mathcal{M}_{ii}|^2 n(\Omega_0) + \sum_f m_f^*|\mathcal{M}_{if}|^2[1+2n(\Omega_0)]\right\}, \tag{22}$$

where m_i^* now denotes the IS electron band mass. The e–p matrix elements between initial (i) and final (f) bands are given by

$$\mathcal{M}_{if} = \int_{-\infty}^{+\infty}\phi_f(z)\left\{\int \frac{\partial V_{ei}}{\partial R_z}(R_z=0;z,\vec{x})\mathrm{e}^{\mathrm{i}(\vec{k}_f-\vec{k}_i)\cdot\vec{x}}\,\mathrm{d}\vec{x}\right\}\phi_i(z)\,\mathrm{d}z. \tag{23}$$

The $\vec{x}$-integration is taken over a circular sheet with a radius given by half the distance between the Na atoms in the monolayer, which corresponds to 3.7 au. This integration was tested by introducing a variable cut-off radius R_{cut} in the $\vec{x}$-integration. In figure 4 we show the result of this test for $\Gamma_{\rm ep}^{QWS}$ at $T = 0$. We conclude that for 0.95 ML of Na the saturated value of 22 meV for $\Gamma_{\rm ep}^{QWS}$ is obtained with $R_{cut} \approx 3$ au. This result justifies the assumption we made to derive equations (21) and (22), namely that interference effects between the vibrating Na ions within the monolayer can be neglected—Na ions vibrate as independent Einstein oscillators with the frequency Ω_0.

For a comparison with normal photoemission experiments for the QWS decay we add to $\Gamma_{\rm ep}$ the contribution from the decay channel due to e–e scattering, $\Gamma_{\rm ee}$, in figure 5. The reported normal photoemission data [43] are taken for 0.95 ML Na on Cu(111). For this coverage the hole binding energy is 80 meV [43]. The calculated mass enhancement factor $\lambda = 0.23$ agrees well with that experimentally determined from the Γ slope versus temperature, $\lambda = 0.22$ [43]. Adding $\Gamma_{\rm ee}$ and $\Gamma_{\rm ep}$ we obtain reasonable agreement with experiment as seen in figure 5.

High-resolution two-photon photoemission measurements have been used to determine the lifetime broadening of the three ISs of the system of 1 ML Na/Cu(111) [21]. The lowest-lying IS was reported to have an FWHM of 140 meV [21]. In figure 6 we show our results for $\Gamma_{\rm ep}$ versus temperature. First of all, in comparison with experiment, the decay of the IS due to absorption or emission of phonons seems unimportant, with less than a 10 meV contribution to the broadening. However, we find that the most efficient decay channel for the excited electron

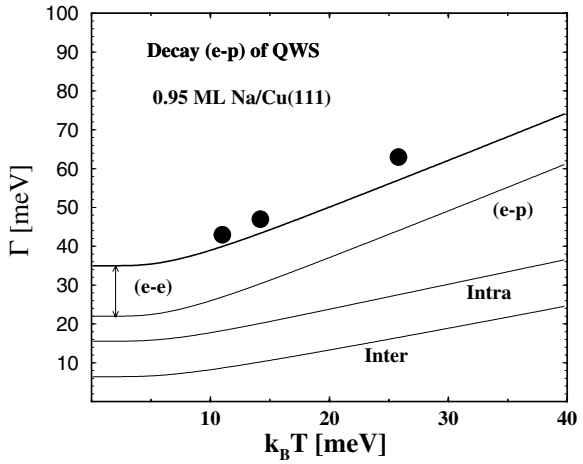

Figure 5. The lifetime broadening of the QWS of 0.95 ML Na on Cu(111) at the $\bar{\Gamma}$-point calculated as a function of temperature. The contribution to Γ_{ep} from intraband and interband scattering is denoted 'Intra' and 'Inter'. These two contributions are given by the first and second terms in equation (21) respectively. The normal photoemission data are from [43] (filled circles). The size of the filled circles corresponds to the experimental resolution of about 5 meV.

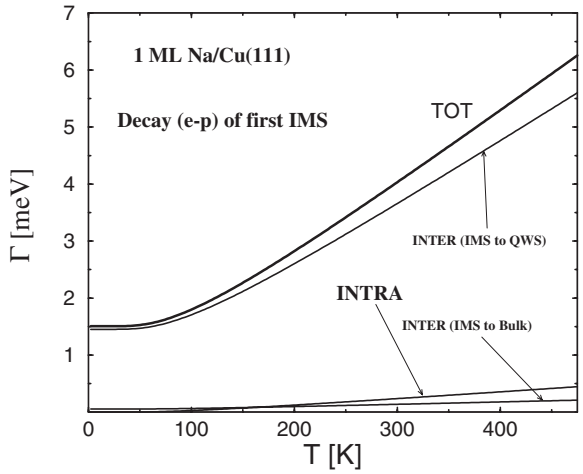

Figure 6. Phonon-induced lifetime broadening of the first IS of 1 ML Na on Cu(111) at the $\bar{\Gamma}$-point calculated as a function of temperature.

is to scatter to the QWS band. The intraband decay or decay to the bulk bands is of minor importance, which is easy to understand considering the e–p matrix elements in equation (23). The greatest overlap between the initial state, deformation potential and final state is when the final state is the QWS. This is illustrated in figure 7. Since the amplitudes of the bulk wavefunctions in the overlap region with the initial IS and the deformation potential are very small, the total contribution from IS $\rightarrow$ bulk states is very small (see figure 6).

We conclude that when comparing the calculated Γ_{ep} for the IS and the QWS, the latter is an order of magnitude greater. The physical reason is that the IS wavefunction has its centre

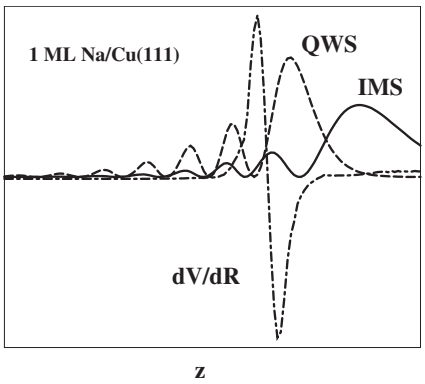

Figure 7. The z-part of the square magnitude of the IS (solid curve) and QWS (dashed curve) wavefunctions. The (x, y)-averaged *ab initio* deformation potential is also shown (dashed–dotted curve).

of gravity further out towards the vacuum in comparison with the wavefunction of the QWS. This yields a much smaller overlap with the deformation potential and the bulk states (in the case of interband scattering). Furthermore, the IS interband transitions are connected with bulk states with much greater parallel momentum, which introduces cancellation effects in the calculation of the e–p matrix elements.

3.3. Noble metal surface states

Several experimental studies of the lifetime broadening of surface states of noble metal surfaces have been reported [19, 36, 41, 42]. Other surfaces with local bandgaps have been studied [18, 40, 53–55] and, in particular, data for the $\bar{\Gamma}$ surface state of Be(0001) indicate an exceptionally strong e–p coupling, $\lambda \approx 0.7$ [57].

We here present results from a recent calculation of the phonon-induced broadening of the intrinsic surface states of the noble metal surfaces Cu(111) and Ag(111) [71]. We want to point out that, in almost all investigations of the e–p interaction, the relevant electron scattering takes place essentially on the Fermi surface and only the Fermi-surface-averaged e–p coupling comes into play. When considering lifetimes of surface states, the situation is quite different. The e–p coupling becomes state dependent as the probed initial electron state is fixed. For the surface states of the studied noble metal surfaces Cu(111) and Ag(111) not only the Fermi surface electron structure is of importance as the binding energy of the initial hole state ranges from 0 (Fermi level) to 0.4 eV. The analysis was based on the calculation of the Eliashberg spectral function $\alpha^2 F(\omega)$ given in equation (8).

The aim was to consider in some detail the phonons, bulk and surface modes. To achieve the phonon dispersion and the phonon polarization vectors we performed a slab calculation according to Black *et al* [72] and expanded the dynamic matrix in Gottleib polynomials [73] to optimize the representation of the surface phonon modes. In figure 8(a) the phonon dispersion for Cu(111) is shown. The low-energy phonon branch is the Rayleigh surface mode, which splits off from the bulk phonon modes.

In comparison with the Na/Cu(111) study described above, we applied a simpler description of the electron–ion potential which determines the deformation potential that drives the electron scattering. We adopted Ashcroft pseudo-potentials [74] as bare electron–ion potentials. We have investigated the screening of the bare potentials by applying the dielectric

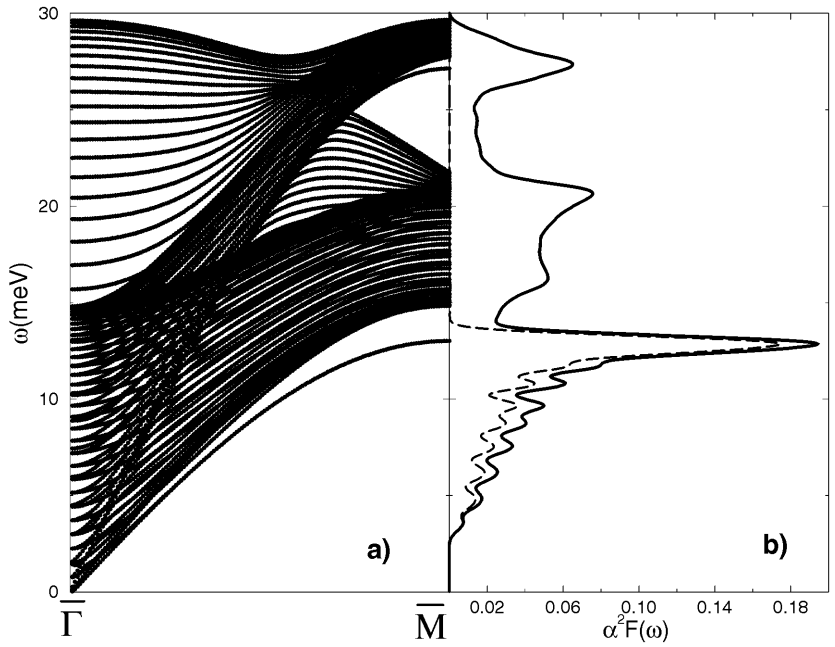

Figure 8. (a) The phonon dispersion from a 31-layer slab calculation in the $\bar{\Gamma}$–$\bar{M}$ direction of the SBZ. (b) The Eliashberg function of the hole state at the $\bar{\Gamma}$ point (solid curve) and the contribution from the Rayleigh mode to the Eliashberg function (dashed curve).

function according to both Thomas–Fermi and RPA (constructed from the eigenwavefunctions and energy eigenvalues from a 31-layer slab calculation). The two different types of screening gave a difference of about 1% for the mass enhancement factor (λ) and the phonon-induced lifetime broadening (Γ_{ep}) due to compensating effects. Referring to the top surface layer, Thomas–Fermi screening is symmetric while RPA yields a screening slightly stronger below and slightly weaker above, due to the asymmetry of the electron density. This is illustrated in figure 9. The one-electron wavefunctions to be used in the calculation of the e–p matrix element in the coupling function g were calculated according to the scheme described in [62–64].

Calculating Γ_{ep} we have to take into account intraband and interband scattering of electrons and also possibly Umklapp processes. For the surface states of the studied noble metals the Umklapp processes can be neglected as the Fermi momenta of the surface states are small ($<$0.12 au) in comparison with half the minimum reciprocal vector ($|\vec{G}|/2 < 0.75$ au). The maximum Fermi momentum vector of the final bulk states, denoted f in figure 10, is $<$0.74 au. Thus, the final hole states are all confined to the first surface Brillioun zone (SBZ). Consequently, Umklapp scattering takes place only for the hole state close to the Fermi level while in the $\bar{\Gamma}$-point we only have normal scattering. In figure 10 we illustrate Umklapp scattering near the Fermi level. We conclude that we can overall neglect the Umklapp processes and approximate by integrating around the complete final-state circle within the first SBZ. We also note that Umklapp processes are only important for small binding energies, but then Γ_{ep} is in any case small at reasonably low temperatures (see equation (11)).

The intraband scattering ($f = i$, in equations (4) and (8)) is neglected for the following reasons. In the case of intraband scattering the parallel momentum of the electron scattered into the hole state is small ($<$0.12 au), in particular when the hole state is close to the $\bar{\Gamma}$-point.

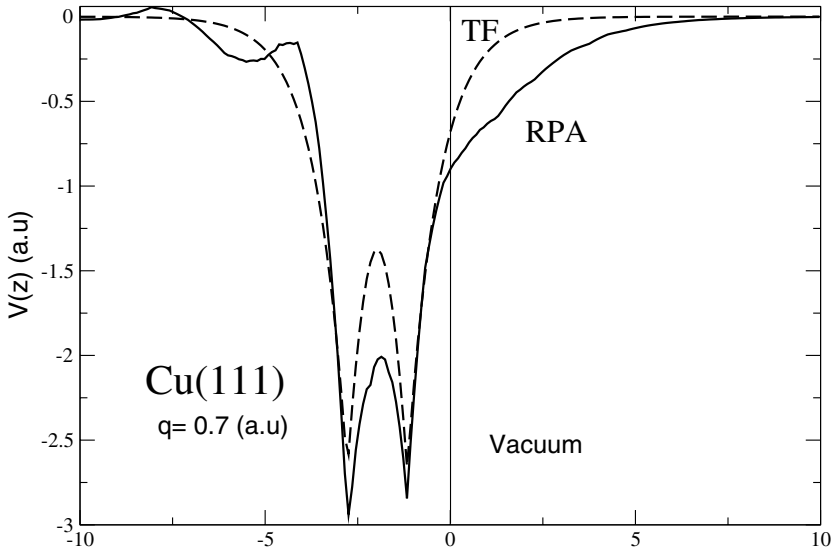

Figure 9. The screened electron–ion potential $\tilde{V}_q^{\mu}(z)$ for the surface layer ($\mu = 1$) as a function of z for Cu(111). Screening according to TF and RPA is shown.

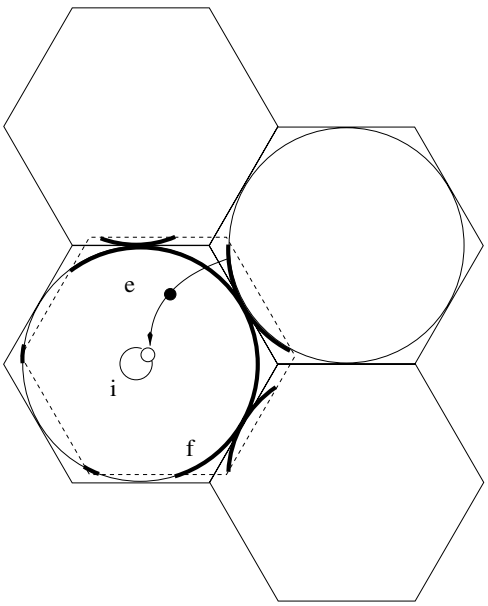

Figure 10. Illustration of the Umklapp processes for Cu(111). The solid hexagons are the surface Brillouin zones in repeated zone scheme. The dashed hexagon is a Brillouin zone centred on the hole (small empty circle). The circle i represents the initial hole state band and the large circle f the maximum final state band. The thick lines on parts of the f circles indicate the possible final state of the hole. One particular scattering event is shown corresponding to an Umklapp process.

This means that the argument for considering only the lowest-order self-energy diagram in figure 1 [48–51] might not be justified. Furthermore, a similar problem is pointed out by Rahman and Mills [75] when they consider the e–p coupling in surface ISs. They illustrate

the breakdown of the golden rule type of expression, equation (7), for the intraband scattering contribution to the lifetime broadening.

However, we argue from a qualitative point of view that the intraband scattering is not as important as the interband scattering. In the case of intraband transitions in the long-wavelength limit, the matrix element of the gradient of the screened electron–ion potential is approximately the expectation value of the force acting on the ions in the direction perpendicular to the surface $\langle \psi_{i,\vec{k}}(\vec{x},z)\vec{\nabla}_{\vec{R}_\mu}\vec{V}^{\mu}(\vec{x},z)\psi_{i,\vec{k}-\vec{q}}(\vec{x},z)\rangle \approx \vec{F}_\mu \approx \langle i|\partial\tilde{V}_0^{\mu}(z)/\partial z|i\rangle\hat{z}$, where μ is a layer index [71]. It is well known that, within a linear response, the sum over the forces acting on the ions induced by an electron (hole) must be zero [76–79], thus the matrix element of the sum of gradients of the screened electron–ion potential is equal to zero, $\sum_\mu \vec{F}_\mu = 0$. Furthermore, the ion displacements forming the phonon modes in the surface region, associated with small q, are locally rigid within a large coherence length of $2\pi/q$ isotropically in all directions, parallel and perpendicular to the surface [80]. For intraband scattering the maximum phonon momentum is about 0.24 au, which corresponds to a coherence length of 26 au, which exceeds the extension of the surface state wavefunction in the direction of the surface normal. Also taking into account the reduced phase space for an intraband scattering process makes the intraband contribution negligible compared with interband scattering.

We now turn to the results of the calculations concerning the hole binding energy and temperature dependence of the studied surface states. The most interesting hole binding energy region is close to the Fermi level, in particular when the binding energy is less than the maximum phonon frequency ω_m. In this region we expect that the lifetime broadening is completely determined by the e–p coupling. The contribution from e–e interaction is very small, for Cu(111) and Ag(111), $\Gamma_{ee} < 0.2$ meV.

In figure 11 we present the calculated Γ_{ep}, at $T = 30$ K, for Cu(111) and Ag(111). Applying a simple Debye model, discussed in section 3.1, we would expect from equation (11) a cubic (three-dimensional Debye model) or a quadratic (two-dimensional Debye model) dependence on the binding energy $|\omega|$, which obviously is not the case. The calculated structure of Γ_{ep} in the small-binding-energy region, seen in figure 11, is determined by the Eliashberg function, which reflects the real phonon density of states of the system. The high-resolution ARPES data show some of these structures [71], indicating the possibility of experimentally obtaining the Eliashberg function at low temperatures. This possibility is of great interest as then the mass enhancement factor λ could be obtained from the first reciprocal moment given by equation (15), without having to measure the high-temperature slope, which could be difficult from an experimental point of view. The break-point of the increase of Γ_{ep} at $\omega = \omega_m$ ($\approx$30 meV for Cu(111) and 20 meV for Ag(111)) is also seen in the experiment [71].

Adding the contribution from the e–e interaction, values close to the experiment are obtained [71]. We note from figure 11 that the contribution from only the Rayleigh surface mode gives about 38% of Γ_{ep} beyond the maximum phonon frequencies, indicating that bulk phonons give most of the contributions in this range. However, for binding energies below the maximum of the Rayleigh mode energy, this mode alone represents on average about 85% of Γ_{ep}. In [71] we demonstrate a good agreement compared with high-resolution ARPES data.

The main signature of the e–p contribution to the lifetime broadening is the temperature dependence. The temperature (T) dependence of Γ_{ep} was calculated for the hole state at the $\bar{\Gamma}$ point for Cu(111) and Ag(111). For binding energies exceeding $k_B T$ we can neglect the temperature dependence of the e–e scattering. To illustrate the T-dependence of the full lifetime broadening we show in figure 12 the constant contribution from Γ_{ee} and the T-dependent Γ_{ep}. The calculated full lifetime broadenings for both Cu(111) and in particular for Ag(111), are in good agreement with the experimental data [71].

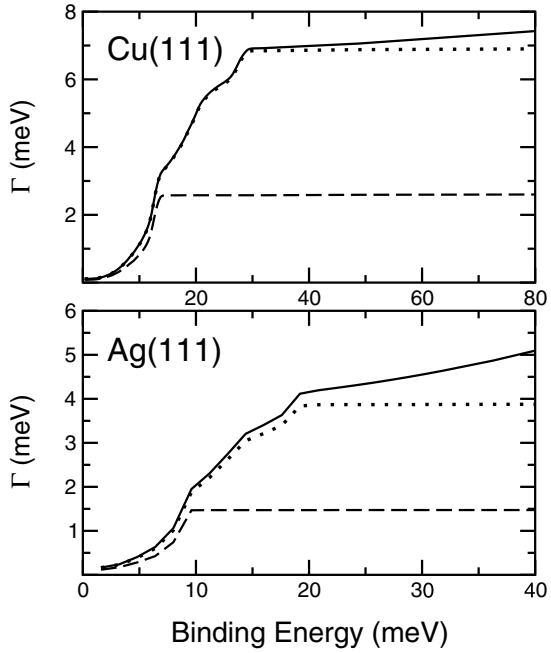

Figure 11. Lifetime broadening of the Cu(111) and Ag(111) surface hole state as a function of binding energy, $\Gamma_{ee} + \Gamma_{ep}$ (solid curve), Γ_{ep} (dotted curve) and Rayleigh mode contribution to Γ_{ep} (dashed curve).

In this study, taking into account realistic phonons made it possible to show the relative importance of bulk and surface modes. The Rayleigh surface phonons are shown to give an important contribution to the phonon-induced lifetime broadening of surface states, in particular for small binding energies. We also demonstrated that, for the description of the e–p scattering, simple Thomas–Fermi screening of Ashcroft pseudo-potentials gives very similar results to a more rigorous RPA screening. We find reasonable agreements with experiments for both the binding energy and temperature dependence of the lifetime broadening.

4. Concluding remarks

In bulk material e–p calculations, the aim is to a large extent a matter of finding a proper deformation potential—the change of the one-electron potential due to the vibrational motion of the ions (phonons). All quantities that determine the e–p coupling matrix element–phonon dispersion relation, phonon polarization vectors, electron wavefunctions and deformation potential—could in principle be obtained from a *first-principles* self-consistent scheme. This is illustrated very nicely in the work by Savrasov *et al* [81], where the Fermi-surface-averaged e–p coupling is studied for several bulk metals applying the density-functional scheme with the linear-muffin-tin-orbital method.

However, to describe the surface state decay presents additional difficulties in a DFT calculation. The super-cell has to include enough vacuum and bulk layers in order to obtain convergence in the summation over final states in equation (7), in other words to obtain the proper Eliashberg spectral function in equation (8). This requires a very large number of layers in the slab. In the calculation of the QWS hole decay (see section 2.2) we found that a slab

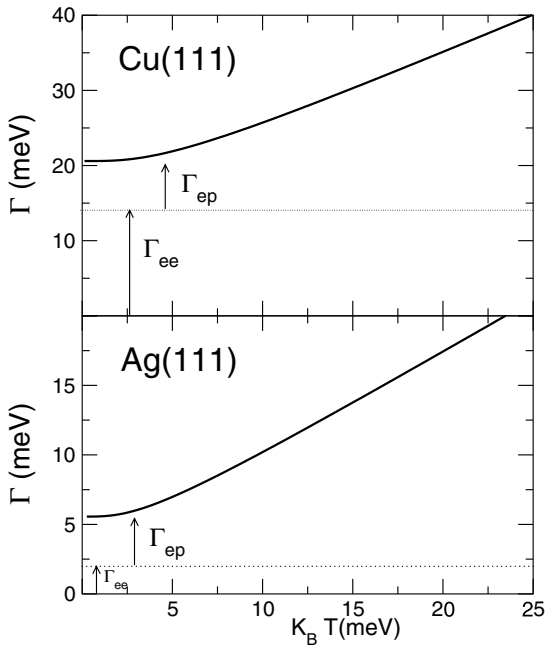

Figure 12. Lifetime broadening of the Cu(111) and Ag(111) surface hole states as a function of temperature (solid curve), Γ_{ee} (dotted line).

corresponding to ≈25 layers is needed [44] and for the hole decay in the surface state bands of Cu(111) and Ag(111), described in section 3.3, a 31-layer slab was used. For this reason a full *first-principles* e–p calculation is hard to execute. However, one can benefit from the fact that the charge density and thus the effective one-electron potential converges typically for a 6–8-layer slab. By inserting a bulk potential, with arbitrary many layers, in the centre of the slab, a single final iteration then produces the desired one-electron states. This method, although not used here, has been successfully applied in recent DFT calculations [82, 83].

We have demonstrated with the presented model calculations that it is possible to reasonably well understand experimental data concerning the e–p-induced lifetime broadening of surface states by taking into account bulk and surface electron and phonon states.

There are many challenging projects for the future, concerning theoretical investigations of the e–p interaction on metal surfaces. To mention a few,

(i) a rigorous theory to calculate the intraband scattering contribution when surface and bulk acoustic phonon modes are present,
(ii) explaining the observed seemingly strong e–p coupling for the multi-overlayer structures, taking into account properly the phonons, and, when it comes to methods,
(iii) full-scale *first-principles* calculations of Γ_{ep}.

Acknowledgments

We acknowledge partial support by the Basque Country Government, the University of the Basque Country, Ministerio de Ciencia y Tecnologia. We also would like to thank P M Echenique for fruitful discussions and L Walldén and S Å Lindgren for valuable comments on the manuscript.

References

[1] Echenique P, Pitarke J, Chulkov E and Rubio A 2000 *Chem. Phys.* **251** 1
[2] Chulkov E V, Silkin V M and Machado M 2001 *Surf. Sci.* **482–485** 693
[3] Borisov A G, Gauyacq J P, Kazansky A K, Chulkov E V, Silkin V M and Echenique P M 2001 *Phys. Rev. Lett.* **86** 488
[4] Brivio G P and Grimley T B 1979 *Surf. Sci.* **89** 226
[5] Persson B and Persson M 1980 *Solid State Commun.* **36** 175
[6] Korzeniewski G E, Hood E and Metiu H 1980 *J. Chem. Phys.* **80** 6274
[7] Persson M and Hellsing B 1982 *Phys. Rev. Lett.* **49** 662
[8] Hellsing B and Persson M 1984 *Phys. Scr.* **29** 360
[9] Hellsing B 1985 *Surf. Sci.* **152–3** 826
[10] Hellsing B 1985 *J. Chem. Phys.* **83** 1371
[11] Rantala T T, Rosén A and Hellsing B 1986 *J. Electron. Spectrosc. Relat. Phenom.* **39** 173
[12] Billing G D 2000 *J. Chem. Phys.* **112** 335
[13] Lindgren S Å and Walldén L 1987 *Phys. Rev. Lett.* **59** 3003
[14] Carlsson A, Claesson D, Lindgren S Å and Walldén L 1996 *Phys. Rev. Lett.* **77** 346
[15] Theilmann F, Matzdorf R, Meister G and Goldmann A 1997 *Phys. Rev.* B **56** 3632
[16] Matzdorf R 1998 *Surf. Sci. Report.* **30** 153
[17] Paggel J, Miller T and Chiang T 1999 *Phys. Rev. Lett.* **83** 1415
[18] Valla T, Fedorov A V, Johnson P D and Hulbert S L 1999 *Phys. Rev. Lett.* **83** 2085
[19] Reinert F, Nicolay G, Schmidt S, Ehm D and Hüfner S 2001 *Phys. Rev.* B **63** 115415
[20] Fischer N, Schuppler S, Fischer R, Fauster Th and Steinmann W 1991 *Phys. Rev.* **43** 14 722
[21] Fischer N, Schuppler S, Fischer R, Fauster Th and Steinmann W 1993 *Phys. Rev.* **47** 4705
[22] Höfer U, Shumay I L, Reuss Ch, Thomann U, Wallauer W and Fauster Th 1997 *Science* **277** 1480
[23] Harris C B, Ge N H, Lingle R L Jr, McNeill J D and Wong C M 1997 *Ann. Rev. Phys. Chem.* **48** 711
[24] Wolf M, Knoesel E and Hertel T 1996 *Phys. Rev.* B **54** R5295
[25] Petek H and Ogawa S 1998 *Prog. Surf. Sci.* **56** 239
[26] Knoesel E, Hotzel A and Wolf M 1998 *J. Electron. Spectrosc. Relat. Phenom.* **88–91** 577
[27] Bauer M, Pawlik S and Aeschlimann M 1999 *Phys. Rev.* B **60** 5016
[28] Ogawa S, Nagano H and Petek H 1999 *Phys. Rev. Lett.* **82** 1931
[29] Schäfer A, Shumay I L, Wiets M, Weinelt M, Fauster Th, Chulkov E V, Silkin V M and Echenique P M 2000 *Phys. Rev.* B **61** 13 159
[30] Link S, Dürr H A, Bihlmayer G, Blügel S, Eberhardt W, Chulkov E V, Silkin V M and Echenique P M 2001 *Phys. Rev.* B **63** 115420
[31] Shen X J, Kwak H, Radojevic A M, Smadici S, Mocuta D and Osgood R M Jr 2002 *Chem. Phys. Lett.* **351** 1
[32] Berthold W, Höfer U, Feulner P, Chulkov E V, Silkin V M and Echenique P M 2002 *Phys. Rev. Lett.* **88** 056805
[33] Roth M, Pickel M, Jinxiong W, Weinelt M and Fauster Th 2002 *Phys. Rev. Lett.* **88** 096802
[34] Li J, Schneider W-D, Berndt R, Bryant O R and Crampin S 1998 *Phys. Rev. Lett.* **81** 4464
[35] Bürgi L, Jeandupeux O, Brune H and Kern K 1999 *Phys. Rev. Lett.* **82** 4516
[36] Kliewer J, Berndt R, Chulkov E V, Silkin V M, Echenique P M and Crampin S 2000 *Science* **288** 1399
[37] Kliewer J, Berndt R and Crampin S 2001 *New J. Phys.* **3** 22.1
[38] Hövel H, Grimm B and Reihl B 2001 *Surf. Sci.* **477** 43
[39] Braun K-F and Rieder K-H 2002 *Phys. Rev. Lett.* **88** 096801
[40] Bauer A, Mühlig A, Wegner D and Kaindl G 2002 *Phys. Rev.* B **65** 075421
[41] Matzdorf R, Meister G and Goldmann A 1993 *Surf. Sci.* **286** 56
[42] McDougall B A, Balasubramanian T and Jensen E 1995 *Phys. Rev.* B **51** 13 891
[43] Carlsson A, Hellsing B, Lindgren S -Å and Walldén L 1997 *Phys. Rev.* B **56** 1593
[44] Hellsing B, Carlsson J, Lindgren S -Å and Walldén L 2000 *Phys. Rev.* B **61** 2343
[45] Paggel J, Miller T and Chiang T 1998 *Phys. Rev. Lett.* **81** 5632
[46] Valla T *et al* 2000 *J. Phys.: Condens. Matter* **12** L477
[47] Kralj M *et al Phys. Rev.* B **64** 085411
[48] Migdal A 1958 *Sov. Phys.–JETP* **7** 996
[49] Rickayzen G 1980 *Green's Functions and Condensed Matter, Techniques of Physics* vol 5, ed N March and H Daglish (London: Academic)
[50] Grimvall G 1981 *The Electron–Phonon Interaction in Metals, Selected Topics in Solid State Physics* ed E Wohlfarth (New York: North-Holland)
[51] Mahan G 1990 *Many-Particle Physics, Physics of Solids and Liquids* ed J Devrees *et al* (New York: Plenum) p 588

[52] McMillan W 1968 *Phys. Rev.* **167** 331
[53] Straube P, Pforte F, Michalke T, Berge K, Gerlach A and Goldmann A 2000 *Phys. Rev.* B **61** 14 072
[54] Silkin V M, Balasubramanian T, Chulkov E V, Rubio A and Echenique P M 2001 *Phys. Rev.* B **64** 085334
[55] Balasubramanian T, Johansson L I, Glans P-A, Virojanadara C, Silkin V M, Chulkov E V and Echenique P M 2001 *Phys. Rev.* B **64** 205401
[56] Balasubramanian T, Jensen E, Wu X and Hulbert S 1998 *Phys. Rev.* B **57** R6866
[57] LaShell S, Jensen E and Balasubramanian T 2000 *Phys. Rev.* B **61** 2371
[58] Kostur V M and Mitrovic B 1993 *Phys. Rev.* B **48** 16 388
[59] Paggel J, Miller T and Chiang T 1999 *Science* **283** 1709
[60] Kröger J, Bruchmann D, Lehwald S and Ibach H 2000 *Surf. Sci.* **449** 227
[61] Benedek G *et al* 1992 *Phys. Rev. Lett.* **69** 2951
[62] Chulkov E V, Silkin V M and Echenique P M 1997 *Surf. Sci.* **391** L1217
[63] Chulkov E, Silkin V and Echenique P 1999 *Surf. Sci.* **437** 330
[64] Chulkov E V, Sarria I, Silkin V M, Pitarke J M and Echenique P M 1998 *Phys. Rev. Lett.* **80** 4947
[65] Carlsson J and Hellsing B 2000 *Phys. Rev.* B **61** 13 973
[66] Hohenberg P and Kohn W 1964 *Phys. Rev.* B **136** 864
[67] Kohn W and Sham L 1965 *Phys. Rev.* B **140** 1133
[68] Perdew J *et al* 1992 *Phys. Rev.* B **46** 6671
[69] Vanderbildt D 1990 *Phys. Rev.* B **41** 7892
[70] Lindgren S -Å and Walldén L 1993 *J. Electron. Spectrosc.* **64/65** 483
[71] Eiguren A, Hellsing B, Reinert F, Nicolay G, Chulkov E V, Silkin V M, Hüfner S and Echenique P M 2002 *Phys. Rev. Lett.* **88** 066805
[72] Black J E and Shanes F C 1983 *Surf. Sci.* **133** 199
[73] Trullinger S 1976 *J. Math. Phys.* **17** 1884
[74] Ashcroft N and Langreth D 1966 *Phys. Rev.* **159** 500
[75] Rahman T S and Mills D L 1980 *Phys. Rev.* B **21** 1432
[76] Sorbello R S and Dasgupta B B 1980 *Phys. Rev.* B **21** 2196
[77] Budd H F and Vannimenus J 1975 *Phys. Rev.* B **12** 509
[78] Andersson S, Persson B N J, Persson M and Lang N 1984 *Phys. Rev.* B **23** 2073
[79] Persson M, Stroscio J A and Ho W 1987 *Phys. Scr.* **36** 548
[80] Flatté M E and Kohn W 1991 *Phys. Rev.* B **43** 7422
[81] Savrasov S Y and Savrasov D Y 1996 *Phys. Rev.* B **54** 16 487
[82] Silkin V M, Chulkov E V and Echenique P M 1999 *Phys. Rev.* B **60** 7820
[83] Silkin V M, Chulkov E V and Echenique P M 2001 *Phys. Rev.* B **64** 172512